2002

Convection in chemical fronts with quadratic and cubic autocatalysis

Desiderio A. Vasquez
vasquez@ipfw.edu

Erik Thoreson
This research is a product of the Department of Physics faculty at Indiana University-Purdue University Fort Wayne.

Convection in chemical fronts with quadratic and cubic autocatalysis

Desiderio A. Vasquez[a)]
Pontificia Universidad Catolica del Peru, Departamento de Ciencias, Seccion Fisica, Apartado 1761, Lima 100, Peru

Erik Thoreson
Department of Physics, Indiana University-Purdue University Fort Wayne, Fort Wayne, Indiana 46805-1499

(Received 3 April 2001; accepted 14 November 2001; published 21 February 2002)

Convection in chemical fronts enhances the speed and determines the curvature of the front. Convection is due to density gradients across the front. Fronts propagating in narrow vertical tubes do not exhibit convection, while convection develops in tubes of larger diameter. The transition to convection is determined not only by the tube diameter, but also by the type of chemical reaction. We determine the transition to convection for chemical fronts with quadratic and cubic autocatalysis. We show that quadratic fronts are more stable to convection than cubic fronts. We compare these results to a thin front approximation based on an eikonal relation. In contrast to the thin front approximation, reaction–diffusion models show a transition to convection that depends on the ratio between the kinematic viscosity and the molecular diffusivity. © *2002 American Institute of Physics.* [DOI: 10.1063/1.1436500]

Autocatalytic reaction fronts propagate in liquids changing the density of the unreacted fluid. This change in density leads to convection as the front propagates upward in a vertical cylinder. Convection sets in as the diameter of the cylinder is increased. The speed and the curvature of the front increase due to convection. Convectionless fronts are flat, propagating with a speed that depends on the type of autocatalysis. We show that the onset of convection as well as the increase of speed also depend on the type of autocatalysis. We compare our results with a thin front approximation that neglects the type of autocatalysis.

I. INTRODUCTION

Autocatalytic reaction fronts generate thermal and concentration gradients that lead to mass density gradients. The density difference between reacted and unreacted fluids generate convection in several chemical reactions. The observed complex behavior varies with the type of chemical reaction. Nagypal *et al.* showed that propagation of chemical waves in the iron(II)–nitric acid reaction depends on the tube orientation.[1] Concentric patterns of precipitation arise in the chlorite–thiourea reaction due to combined effects of the chemical reaction and convection.[2,3] Sakurai and co-workers found an oscillatory surface deformation coupled to convection in a spiral wave train in the Belousov–Zhabotinskii reaction.[4] Komlosi and collaborators observed convective fluid motion in the Belousov–Zhabotinskii reaction inside a vertical tube.[5] A series of detailed experiments by Masere *et al.* in the iodate–arsenous acid reaction showed that convection increases the front speed and changes the curvature of the front.[6] In those experiments, a front was initiated inside a vertical capillary tube. As the front propagates upward, the heavier unreacted fluid is placed above a lighter reacted fluid, convection sets in for tubes of diameters larger than a critical diameter. Fronts propagating downward do not exhibit convection. Near the transition to convection the front is nonaxisymmetric, with fluid rising on one side of the tube, and falling on the opposite side. Away from convection the front is axisymmetric with fluid rising through the middle of the tube and falling on the sides.

The complex behavior observed in the different chemical reactions is caused by the interaction between molecular diffusion, an autocatalytic reaction, and buoyancy. The propagation of the convectionless front is caused by the interaction between molecular diffusion and autocatalysis. A certain chemical is transported through diffusion, for which the autocatalytic reaction generates more of it. Therefore a chemical front appears. If convection is present, buoyancy leads to fluid motion, with an enhancement of mixing, facilitating the faster propagation of the front. This problem is reminiscent of the Rayleigh–Taylor problem where two immiscible fluids are placed one on top of the other, with the heavier fluid on top. However, this problem is different than the Rayleigh–Taylor problem since the front is stabilized by the curvature dependence of the interface velocity, not by surface tension.[7] As a consequence of this relation, the molecular diffusivity determines a critical wave number for the onset of convection, which does not appear in the Rayleigh–Taylor problem.[7]

Previous theoretical studies for convection in autocatalytic reactions where carried out for the Belousov–Zhabotinskii reaction and for the iodate–arsenous acid reaction. The Belousov–Zhabotinskii reaction was modeled using a standard Oregonator model describing a wave of chemical activity on an excitable media, with density driven convection modifying the shape of the wave and increasing the speed of the front.[8,9] Theoretical studies of convection

[a)]Permanent address: Department of Physics, Indiana University-Purdue University Fort Wayne, Fort Wayne, IN 46805-1499.

driven by surface tension gradients (Marangoni-type convection) explained experimental velocity profiles.[10] The iodate–arsenous acid reaction leads to a reaction front propagating on an unreacted solution. The reacted mixture does not allow the passage of multiple waves as in the Belousov–Zhabotinskii reaction, therefore the chemical front can be modeled with a thin front approximation where all the chemical reaction takes place in a very narrow region near the front.[11] However, the results of the thin front approximation are different from the results of the more detailed reaction–diffusion model as the front curvature increases.[12] This indicates that the explicit reaction mechanism plays an important role in the description of chemical waves involving convection. In this paper, we will compare the effects of convection on fronts with two different types of reaction mechanism: quadratic and cubic autocatalysis. Fronts with quadratic autocatalysis were used by Fisher as models of wave behavior in biological systems.[13] These fronts were formally studied independently by Kolmogorov *et al.*[14] The fronts with cubic autocatalysis were successfully applied to fronts in the iodate–arsenous acid reaction.

II. EQUATIONS OF MOTION

We analyze two types of autocatalytic chemical reactions.[15] A quadratic chemical autocatalysis,

$$A+B\rightarrow 2B, \quad \text{rate}=k_q ab,$$

and a cubic chemical autocatalysis,

$$A+2B\rightarrow 3B, \quad \text{rate}=k_c ab^2.$$

We also consider mixed-order autocatalysis where the rate law is a linear combination of both types. Since the net reaction is $A\rightarrow B$, the sum of concentrations must be equal to the initial concentrations $a+b=a_0+b_0$. The initial medium corresponds to $b_0=0$ with a localized initial perturbation to trigger the chemical front. Using this fact and coupling to molecular diffusion in a fluid with a local velocity $\vec{V}$, we obtain an advection–reaction–diffusion equation on the concentration a,

$$\frac{\partial a}{\partial t}+(\vec{V}\cdot\nabla)a=D\nabla^2 a-k_q a(a_0-a)-k_c a(a_0-a)^2. \quad (1)$$

In this paper we seek numerical solutions to the reaction–diffusion–convection problem by coupling hydrodynamic equations for fluid flow to the reaction–diffusion model. We consider two types of fluid flow: flow in porous media and viscous flow. The former is described using Darcy's law

$$\vec{V}=-\frac{k}{\rho_0\nu}(\vec{\nabla}P+\rho g\hat{z}), \quad (2)$$

while flow in viscous fluid is described with the Navier–Stokes equations

$$\frac{\partial\vec{V}}{\partial t}+(\vec{V}\cdot\nabla)\vec{V}=-\frac{1}{\rho_0}\nabla P-\frac{\rho}{\rho_0}g\hat{z}+\nu\nabla^2\vec{V}. \quad (3)$$

In these equations $\vec{V}$ is the fluid velocity, P is the pressure, ρ_0 is the mass density of the unreacted fluid, ν is the kinematic viscosity, g is the magnitude of the acceleration of gravity, $\hat{z}$ is a unit vector pointing parallel to the gravitational field directed upward, k is the coefficient of permeability of the porous medium. We assume that the density (ρ) varies linearly with concentration

$$\rho=\rho_0(1+\delta\alpha), \quad (4)$$

here the parameter δ represents the fractional density difference between reacted and unreacted fluid, and the variable α represents the ratio of the concentration a to the initial concentration a_0. Note that $\alpha=0$ corresponds to the lighter reacted fluid, while $\alpha=1$ is the concentration for the heavier unreacted fluid. The front is set to propagate vertically upward.

In both cases we assume that the density difference affects only the large gravity term; therefore, the continuity equation is reduced to

$$\nabla\cdot\vec{V}=0. \quad (5)$$

This allows to use the stream function (ψ) as it relates to the velocity components in two dimensions:

$$V_x=\frac{\partial\psi}{\partial z} \quad \text{and} \quad V_z=-\frac{\partial\psi}{\partial x}. \quad (6)$$

With this substitution, Darcy's law becomes

$$\nabla^2\psi=\frac{kg}{\nu\rho_0}\frac{\partial\rho}{\partial x}, \quad (7)$$

and the Navier–Stokes equations can be written as

$$\frac{\partial\omega}{\partial t}=\frac{\partial(\psi,\omega)}{\partial(x,z)}+\nu\nabla^2\omega+\frac{g}{\rho_0}\frac{\partial\rho}{\partial x}, \quad (8)$$

with the vorticity ω defined as

$$\omega=\nabla^2\psi, \quad (9)$$

and for two functions f_1 and f_2 we defined

$$\frac{\partial(f_1,f_2)}{\partial(x,z)}=\frac{\partial f_1}{\partial x}\frac{\partial f_2}{\partial z}-\frac{\partial f_1}{\partial z}\frac{\partial f_2}{\partial x}. \quad (10)$$

We write the equations of motion in dimensionless form using $t_{ch}=(k_q a_0+k_c a_0^2)^{-1}$ as unit of time, $L=(Dt_{ch})^{1/2}$ as unit of length, D as unit of the stream function, D/L^2 as unit of the vorticity, the parameter $\mu=k_q/(k_q+k_c a_0)$, the dimensionless concentration $\alpha=a/a_0$,

$$\frac{\partial\omega}{\partial t}=\frac{\partial(\psi,\omega)}{\partial(x,z)}+\mathrm{S}_c\nabla^2\omega+\mathrm{RaS}_c\frac{\partial\alpha}{\partial x}, \quad (11)$$

and

$$\frac{\partial\alpha}{\partial t}=\frac{\partial(\psi,\alpha)}{\partial(x,z)}+\nabla^2\alpha-\mu\alpha(1-\alpha)-(1-\mu)\alpha(1-\alpha)^2. \quad (12)$$

We defined a dimensionless Rayleigh number

$$\mathrm{Ra}=\frac{g\,\delta L^3}{\nu D} \quad (13)$$

and a dimensionless Schmidt number

$$S_c = \frac{\nu}{D}. \tag{14}$$

For flow in porous media, the Navier–Stokes equations [Eq. (8)] are replaced by Darcy's law,

$$\nabla^2 \psi = \mathrm{Ra}_p \frac{\partial \alpha}{\partial x}. \tag{15}$$

Here the equivalent Rayleigh number (Ra_p) for flow in porous media corresponds to

$$\mathrm{Ra}_p = \frac{kgL\,\delta}{\nu D}. \tag{16}$$

The convectionless equations ($\vec{V}=0$) with pure cubic autocatalysis ($\mu=0$) have an analytical solution in one dimension where a chemical front propagates with a speed equal to $1/\sqrt{2}$. In the case of quadratic autocatalysis ($\mu=1$) there is no analytical solution, numerical solutions where the initial conditions have compact support lead to fronts with speed equal to 2.[15]

The full set of equations are solved using no flow boundary conditions for the chemical concentration and free boundary conditions for the velocity field. This choice of boundary conditions is required for flows described with Darcy's law. For viscous fluids the natural set of boundary conditions require zero velocity at the walls. However, since our goal is to compare both types of fluid motion we set both boundary conditions to free boundaries where only the normal component of the velocity vanishes.

III. NUMERICAL METHODS

The equations of motion are solved numerically using a finite difference scheme on a two-dimensional grid. The spatial region represents the projection of a vertical cylinder on a two-dimensional plane. A complete solution requires a three-dimensional solution in a cylindrical geometry. However, previous studies of two-dimensional models have proved valuable in understanding experimental observations. Studies in a vertical slab showed a transition to convection as the slab width is increased, a nonaxisymmetric front near the onset of convection, an increase of speed of the front due to convection, and a subsequent transition to axisymmetric fronts.[6,16,17] These effects where observed in experiments as well as in three-dimensional models. Therefore, we can gain valuable insights solving the equations in two dimensions. The spatial variables are discretized using five points for the two-dimensional Laplacian operator (∇^2), and a second order approximation for the first derivatives. The grid size is $\Delta z = 0.35$ dimensionless units for the vertical direction, using 200 grid points for the vertical direction gives a slab of length 70. This choice of grid approximates very well analytic solutions for convectionless fronts. Our calculations are carried out for different widths, the grid size is kept near $\Delta x = 0.133$. The number of points in the horizontal domain is varied to accommodate slabs of different width. More points for wider slabs, less for narrower slabs. We tested varying the horizontal grid size with no significant change in the results. The Poisson equation [Eq. (9)] is solved using the GENBUN subroutine from the FISHPACK software package.[18] GENBUN provides a direct solution for the Poisson equation using a cyclic reduction algorithm. This method also allows to compute the limit for infinite Schmidt number, where Eq. (11) becomes

$$\nabla^2 \omega + \mathrm{Ra} \frac{\partial \alpha}{\partial x} = 0. \tag{17}$$

The time derivatives are calculated using a finite time step. This allows to compute the concentration and the stream function at a later time step. The procedure is repeated several times to arrive at a steady state. This method is the forward Euler method for time evolution.[19] In these equations, the forward Euler method is effective for flow in porous media and for viscous flow as long as the Schmidt number is small. However, in the iodate–arsenous acid reaction the kinematic viscosity is equal to 9.2×10^{-3} cm^2/s,[7] and the diffusion coefficient 2×10^{-5} cm^2/s, resulting in a Schmidt number of 460. These values require a very small time step to avoid numerical instabilities with the forward Euler method. To calculate flows with large Schmidt numbers, the Laplacian in the Navier–Stokes equations is evaluated implicitly at the next time step. This method leads to an additional Poisson equation that is solved again with the GENBUN program.

For calculations near the onset of convection, we replaced the two-dimensional grid with a one-dimensional grid plus a truncated Fourier expansion on the concentrations and the stream function. This method is similar to the method used by Wu *et al.* resulting in a much faster computation of the critical Rayleigh number without losing accuracy.[17] We utilized this method to calculate the increase of speed near the onset of convection.

In a typical calculation, the reaction front is started by setting the concentration α to a small random number near the bottom of the domain. In the rest of the domain the concentration α is set to one, which corresponds to the concentration of the unreacted fluid. As the front propagates upward, the reaction eventually reaches the other end of the slab. To sustain a steady traveling state, the front is shifted backward as it propagates towards the end of the slab, then the slab is filled with unreacted fluid as it was carried out in Refs. 17 and 20. In this manner, we keep the front near the center of the slab (approximately within 15% of the center).

IV. RESULTS

To calculate the critical Rayleigh number for a transition to convection we introduce small perturbations to an initial convectionless front. If the perturbations died, the front is stable, but if they grow the front is unstable to convection. The critical Rayleigh number for a transition to convection depends on the slab width in dimensionless units. The typical value for the length scale (L) in the iodate–arsenous acid reaction is 3.33×10^{-3} cm, where convection occurs in tubes of radii close to 5×10^{-2} cm (15 in dimensionless units).[21] We describe the time evolution of chemical fronts in a vertical slab of width equal to four, which is below the experimental width but provides us an intermediate regime to show

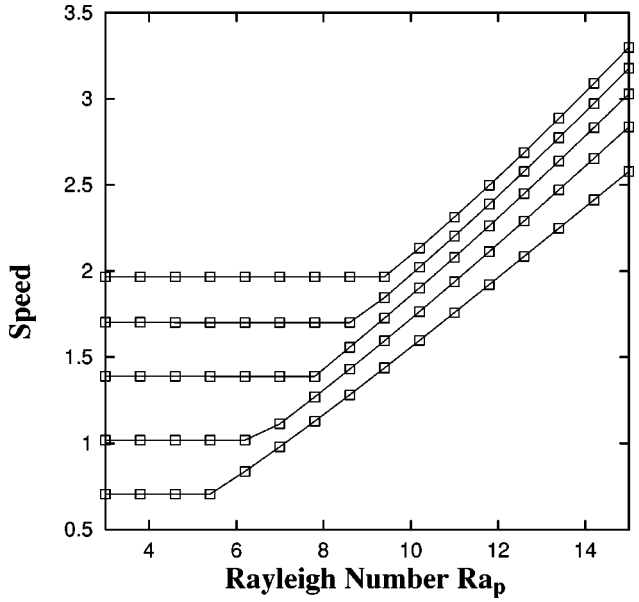

FIG. 1. Increase of speed near the onset of convection as a function of the Rayleigh number. The lines correspond to values of $\mu = 1.0$, 0.75, 0.5, 0.25, and 0.0 from top to bottom. The flow is for a fluid in porous media.

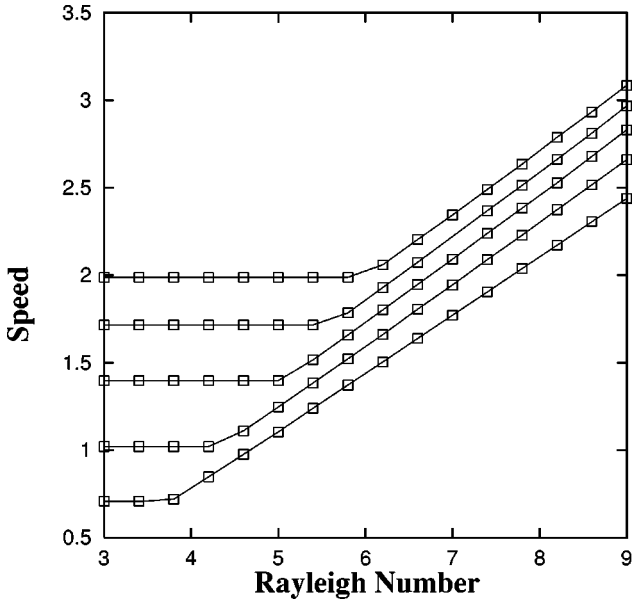

FIG. 2. Increase of speed near the onset of convection as a function of the Rayleigh number. The lines correspond to values of $\mu = 1.0$, 0.75, 0.5, 0.25, and 0.0 from top to bottom. The flow is for a viscous fluid.

our calculations. In a slab of large width, the front thickness is comparatively thin, where the opposite is true in a narrow slab. Our results for slabs of width four are summarized in Fig. 1 where we plot the steady state velocity for different Rayleigh numbers and different types of autocatalytic reactions propagating in a porous media. A purely cubic reaction corresponds to the lowest curve in Fig. 1. For small Rayleigh numbers ($\mathrm{Ra}_p < 5.4$) convection is not present for the cubic fronts. Their speed is equal to $1/\sqrt{2}$, the convectionless speed. As the value of the Rayleigh number (Ra_p) is increased above 5.4, convection sets in, and the speed of the front is increased. The shape of the front is nonsymmetric, with fluid rising on one side of the slab, and falling on the opposite side. For purely quadratic fronts the situation is similar, however the critical Rayleigh number (Ra_p) for the onset of convection is increased to 9.6. Below this critical Rayleigh number the front is flat with speed equal to 2, the speed for convectionless quadratic fronts. As the Rayleigh number is increased, the front speed is also increased. The other lines in Fig. 1 indicate the increase of speed for mixed autocatalysis ($\mu = 0.25$, 0.5, and 0.75, respectively). Near the onset of convection the speed of the front increases almost linearly as a function of the Rayleigh number. The lines near the onset of convection are almost parallel, thus the increase of speed is proportional to the difference between the Rayleigh number and the critical Rayleigh number.

In Fig. 2 we show the results for the speed of autocatalytic reactions in viscous fluids in the limit of infinite Schmidt number. This limit approximates the experimental value of the Schmidt number in the iodate–arsenous acid reaction. The calculations were carried out for slabs of width 4, the same dimensionless width as the previous calculations in porous media. As in the case of flow in porous media, we find convectionless front speeds for Rayleigh numbers below critical values. We also find that the critical Rayleigh numbers for onset of convection depends on the type of autocatalysis. The Rayleigh number for pure cubic autocatalysis ($\mathrm{Ra} = 3.7$) is smaller than for quadratic autocatalysis ($\mathrm{Ra} = 6.0$). Intermediate values indicate that the critical Rayleigh number increases as the parameter μ is increased (μ determines the amount of the type of autocatalysis in the reaction). The results may lead to believe that the critical Rayleigh number for viscous fluids is smaller than for porous media. However, such comparison is not possible since the Rayleigh number for porous media (Ra_p) is different than the Rayleigh number for viscous fluids (Ra). The former has an explicit dependence on k, the permeability.

The results for the critical Rayleigh number as a function of the type of autocatalysis (μ) are shown in Fig. 3 for flow in porous media, and in Fig. 4 for viscous fluids. The figures show the dependence on μ for slabs of different widths. In all those cases, the critical Rayleigh number increases monotonically as a function of μ. This shows that quadratic autocatalytic fronts are more stable to convection as compared to cubic autocatalytic fronts since they require a larger Rayleigh number to begin convection. This result holds for both types of flow, namely viscous fluids and flow in porous media. Another important characteristic in both cases is that the critical Rayleigh numbers for narrow slabs are always larger than for wider widths, indicating that convection is easier to initiate as the fluid is less confined. The figures also indicate that the type of autocatalysis is more important in determining the value of the critical Rayleigh number in narrow slabs. For slabs of width two, the critical Rayleigh number (Ra_p) changes from 17.9 for cubic autocatalysis to 25.5 for quadratic autocatalysis. This range is wider than for slabs of width six, from 2.8 for cubic to 6.1 for quadratic. These conclusions also hold for flow in viscous fluids, were the effects of the type of autocatalysis on the critical Rayleigh number are more pronounced than in narrower slabs.

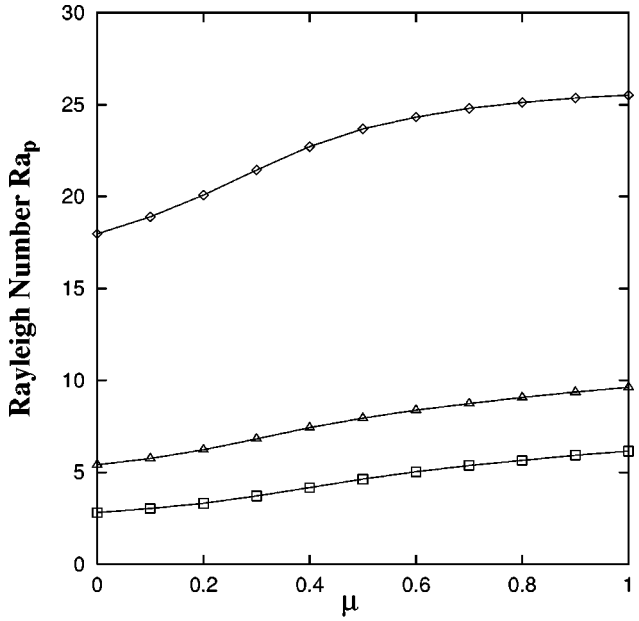

FIG. 3. The critical Rayleigh number as a function of mixing parameter μ. The diamonds correspond to a fluid propagating in a slab of width two, the triangles for a width four, and the squares for a width six. The widths are in dimensionless units. The flow is for a fluid in porous media.

In Fig. 5 we show the variation of the critical Rayleigh number in viscous fluids for slabs of different widths. As was the case in porous media, the critical Rayleigh number decreases as the width of the slab is increased for quadratic and cubic autocatalytic fronts. The fractional difference between Rayleigh numbers for cubic and quadratic autocatalysis increases from about 35% for a slab of width one to 100% for a slab of width 10. In this figure we compare these critical Rayleigh numbers with the ones obtained using a thin front approximation. In the thin front approximation the chemical

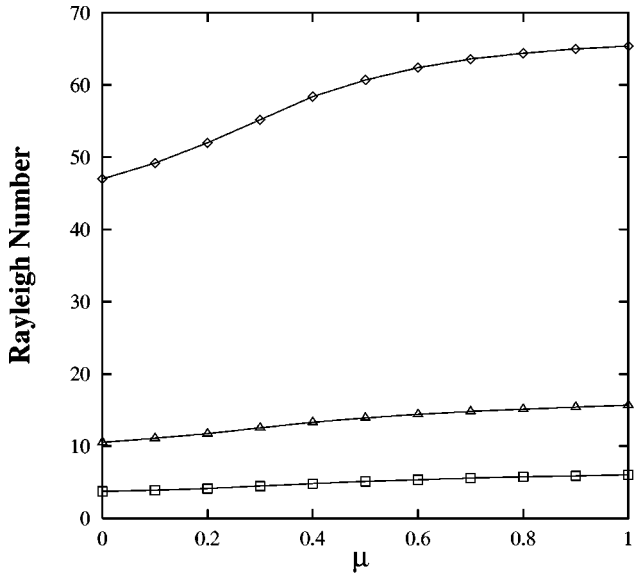

FIG. 4. The critical Rayleigh number as a function of mixing parameter μ. The diamonds correspond to a fluid propagating in a slab of width two, the triangles for a width three, and the squares for a width four. The widths are in dimensionless units. The flow is for a viscous fluid.

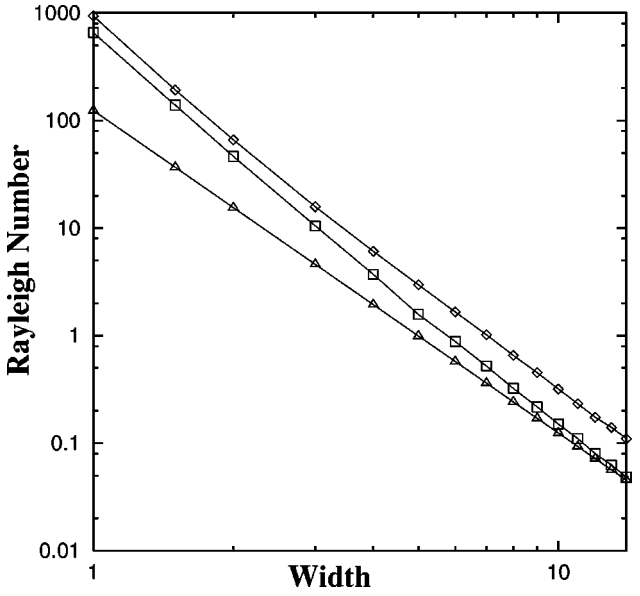

FIG. 5. The critical Rayleigh number for slabs of different widths. The diamonds correspond to quadratic autocatalysis. The squares correspond to cubic autocatalysis, and the triangles correspond to the thin front approximation. The flow is for a viscous fluid.

reaction takes place in a very narrow region near the front. The stability of the front is provided by an eikonal relation between the speed of the curved front to the speed of the flat front. The dependence of the speed on the curvature is proportional only to the diffusion coefficient; it does not include the type of chemical reaction. The results for viscous fluids[7] gives a critical wave number for the onset of convection equal to

$$q_c = \left(\frac{\delta g}{4 \nu D} \right)^{1/3}$$

in conventional units. Using the definition of the Rayleigh number and $q_c = \pi / x_c$, the relation of the critical wave number to x_c, the critical slab width, we obtain the Rayleigh number from the eikonal relation in our dimensionless units:

$$\mathrm{Ra} = 4 \left(\frac{\pi}{x_c} \right)^3 .$$

Our results indicate that the critical Rayleigh number for fronts with cubic autocatalysis approaches the thin front limit for slab widths close to 10. This is not the case for fronts with quadratic autocatalysis as Fig. 5 shows. This result is important since the derivation of the thin front approximation is independent of the type of autocatalysis.[22,23]

Another important result of our calculations is the dependence of the critical Rayleigh number on the Schmidt number, which is the ratio between ν, the kinematic viscosity, and D, the molecular diffusivity. Previous theoretical works using the thin front approximation did not observed this effect, the critical Rayleigh number depended weakly on the speed of the front. This dependence was neglected in studies of the iodate–arsenous acid reaction. Studies of the reaction–diffusion models also focused on the iodate–arsenous acid reaction, where the Schmidt number is large, with the results being close to the limit of infinite Schmidt

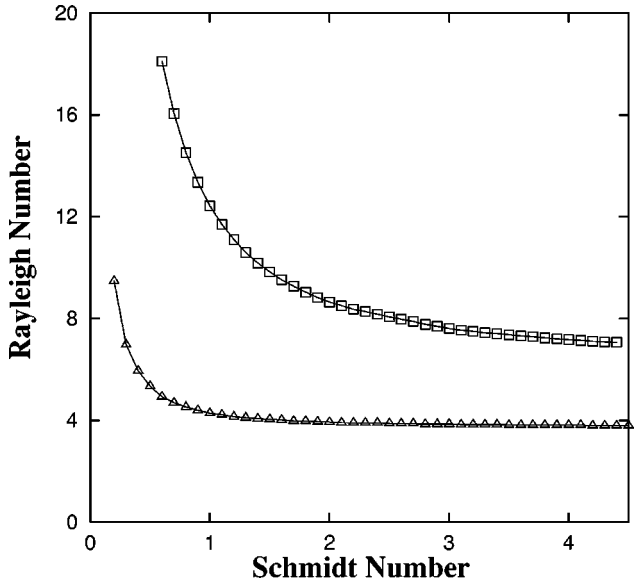

FIG. 6. The critical Rayleigh number as a function of the Schmidt number. The width of the slab is equal to four.

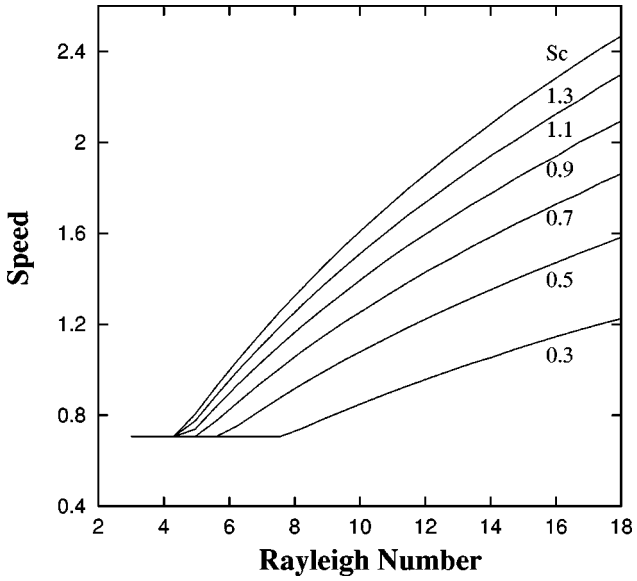

FIG. 7. The increase of speed as a function of Rayleigh number for different values of the Schmidt number. The width of the slab is equal to four. The flow is for a viscous fluid.

number. Our current calculation separates the problem of convection in autocatalytic fronts to the Rayleigh–Benard problem. In the Rayleigh–Benard experiment, convection is set in a layer of fluid heated from below. Convection occurs when the Rayleigh number is raised above a critical value. The Rayleigh number for thermal convection is similar to the viscous Rayleigh number for autocatalytic fronts where the molecular diffusivity is replaced by the thermal diffusivity, and the chemical length scale L is replaced by the thickness of the fluid layer. In the Rayleigh–Benard problem, convection is determined only by the value of the Rayleigh number. In the autocatalytic reaction front, convection is determined by both, the Schmidt number and the Rayleigh number. This fact implies that the critical Rayleigh number for the onset of convection depends on the Schmidt number. This relation is shown in Fig. 6 where we plot the value of the critical Rayleigh number as a function of the Schmidt number for quadratic and cubic autocatalytic fronts. The width of the slab in these calculations is set to four. The critical Rayleigh number is large when the Schmidt number is small for both types of autocatalysis; consequently, the reaction–diffusion front is very stable. This situation can be achieved with a large diffusion coefficient providing stability to the front. For large Schmidt numbers, the critical Rayleigh number approaches a constant limit. The large Schmidt number limit in the cubic autocatalytic reaction is lower than the limit for the quadratic autocatalytic reaction. This limiting situation is closer to the experimental values in the iodate–arsenous acid reaction where the Schmidt number is equal to 460.

The Schmidt number not only affects the onset of convection, but it also determines the rate at which the speed increases once convection sets in. In Fig. 7, we show the speed of the cubic autocatalytic front as the Rayleigh number is increased. We notice that the speed of the front corresponds to the convectionless front for values below the critical Rayleigh number. As the Rayleigh number is increased beyond the critical value, the flat front becomes unstable, convection sets in, and the speed of the front increases. The critical Rayleigh number decreases as the Schmidt number increases, as was also noticed in Fig. 6. The increase of speed for fronts with the Rayleigh number above the critical value is higher for larger Schmidt numbers. This fact is also consistent with our observation that the fronts are more stable to convection if the diffusion coefficient is large, not only the critical Raleigh number is higher, but the increase of speed due to convection is smaller.

V. CONCLUSIONS

The explicit role of the reaction term in explaining convection in autocatalytic fronts cannot be ignored, since different types of autocatalysis lead to different results for the critical Rayleigh number and the increase in front speed. We found that fronts with a quadratic autocatalysis are more stable to convection than fronts with cubic autocatalysis since they require a larger Rayleigh number for convection to set in. This also extends to the case of mixed reactions, the more quadratic the character of the reaction, the more stable the front. In narrow slabs, where the slab width is comparable to the chemical length L, the Rayleigh number is significantly different from the one obtained with a thin front limit. The thin front approximation is a good approximation for fronts with cubic autocatalysis propagating in wider slabs (about 10 times the chemical length). Fronts with quadratic autocatalysis did not approach the thin front limit for the same widths. Another important result of this work is the dependence of convection on the Schmidt number, converging to a constant value at the large Schmidt number limit.

ACKNOWLEDGMENT

This research was supported by a grant from Research Corporation.

[1] I. Nagypal, G. Bazsa, and I. R. Epstein, J. Am. Chem. Soc. **108**, 3635 (1986).
[2] C. R. Chinake and R. H. Simoyi, J. Phys. Chem. **97**, 11569 (1993).
[3] B. S. Martincigh, C. R. Chinake, T. Howes, and R. H. Simoyi, Phys. Rev. E **55**, 7299 (1997).
[4] T. Sakurai, E. Yokoyama, and H. Miike, Phys. Rev. E **56**, R2367 (1997).
[5] A. Komlosi, I. P. Nagy, G. Bazsa, and J. A. Pojman, J. Phys. Chem. **102**, 9136 (1998).
[6] J. Masere, D. A. Vasquez, B. F. Edwards, J. W. Wilder, and K. Showalter, J. Phys. Chem. **98**, 6505 (1994).
[7] B. F. Edwards, J. W. Wilder, and K. Showalter, Phys. Rev. A **43**, 749 (1991).
[8] Y. Wu, D. A. Vasquez, J. W. Wilder, and B. F. Edwards, Phys. Rev. E **51**, 1119 (1995).
[9] D. Zhang, W. R. Peltier, and R. L. Armstrong, J. Chem. Phys. **103**, 4069 (1995).
[10] K. Matthiessen, H. Wilke, and S. C. Muller, Phys. Rev. E **53**, 6056 (1996).
[11] J. W. Wilder, D. A. Vasquez, B. F. Edwards, and G. I. Sivashinsky, Physica D **73**, 217 (1994).
[12] D. A. Vasquez, Phys. Rev. E **56**, 6767 (1997).
[13] R. A. Fisher, Ann. Eugenics **7**, 355 (1937).
[14] A. Kolmogorov, I. Petrovsky, and N. Piscounoff, Bull. Univ. Moscou, Ser. Int., Sect. A **1**, 1 (1937).
[15] S. K. Scott and K. Showalter, J. Phys. Chem. **96**, 8702 (1992).
[16] D. A. Vasquez, J. W. Wilder, and B. F. Edwards, Phys. Fluids A **4**, 2410 (1992).
[17] Y. Wu, D. A. Vasquez, B. F. Edwards, and J. W. Wilder, Phys. Rev. E **52**, 6175 (1995).
[18] R. Sweet, SIAM (Soc. Ind. Appl. Math.) J. Numer. Anal. **14**, 706 (1977); J. Adams, P. Swarztrauber, and R. Sweet, *FISHPACK* (The National Center for Atmospheric Research, Boulder, 1980).
[19] W. H. Press, S. A. Teukolsky, W. T. Vetterling, and B. P. Flannery, *Numerical Recipes in Fortran*, 2nd ed. (Cambridge University Press, Cambridge, 1992).
[20] D. A. Vasquez, J. M. Littley, J. W. Wilder, and B. F. Edwards, Phys. Rev. E **50**, 280 (1994).
[21] A. Saul and K. Showalter, in *Oscillations and Traveling Waves in Chemical Systems*, edited by R. J. Field and M. Burguer (Wiley, New York, 1985), p. 419.
[22] J. W. Wilder, D. A. Vasquez, and B. F. Edwards, Phys. Rev. E **47**, 3761 (1993).
[23] J. P. Keener and J. J. Tyson, Physica D **21**, 307 (1986).